Energy, Volume 242, March 2022, Article number 123030
DOI:10.1016/j.energy.2021.123030

Self-enhancing model-based control for active transient protection and thrust response improvement of gas turbine aero-engines

Zhiyuan Wei [a], Shuguang Zhang [a]*, Soheil Jafari [b], Theoklis Nikolaidis [b]

a. School of Transportation Science and Engineering, Beihang University, Beijing 102206, China
b. Centre for Propulsion Engineering, School of Aerospace Transport and Manufacturing, Cranfield University, Bedfordshire MK43 0AL, UK

* Corresponding author.

Email: gnahz@buaa.edu.cn (S. Zhang)

Abstract

A self-enhancing active transient protection (SeATP) control approach using model-based strategies is proposed for gas turbine aero-engines, which aims at pro-actively handling engine's transient safety limits (i.e. surge margin limit and turbine entry temperature limit) and thrust response improvement over the life cycle. The feature of SeATP is a bank of self-enhancing loops with periodically updated controller parameters for different flight cycles. This is realized by an off-line gain tuning via global optimization approach. Additionally, a sensor-based baseline controller and a model-based active transient protection (ATP) controller (with fixed gains) are developed as comparison bases. Numerical simulations for the examined controllers are carried on a validated aero-thermal turbofan engine model for idle to full-power acceleration tests in Matlab/Simulink environment. Simulation results demonstrate that ATP controller owns a considerable thrust response improvement for both the new engine and a severely degraded engine, compared with the baseline controller. Moreover, the proposed SeATP controller ensures a 65.77% recovery rate of thrust response

deviation caused by the ATP controller for the degraded engine. Particularly, a low transient surge margin trajectory and a high turbine entry temperature route are fulfilled by the SeATP controller. SeATP controller also shows better robustness performance for degradation variation than ATP controller. Hence, the control performance of the SeATP controller is confirmed.

Keywords

Self-enhancing active transient protection, model-based control, gas turbine aero-engine, performance improvement, degradation

Nomenclature

Accel	acceleration
ATP	active transient protection
BR	boost rate
Decel	deceleration
EPR	engine pressure ratio
F	thrust
FAR	fuel-to-air ratio
FC	flight cycle
HPC	high-pressure compressor

HPT	high-pressure turbine
HWM	Hybrid Wiener model
IFB	integrator feedback
ISA	international standard atmosphere
LPT	low-pressure turbine
N1	low-pressure shaft speed
N2	high-pressure shaft speed
N2dot	high-pressure rotor acceleration rate
P3	compressor discharge pressure
PI	proportional-integral
PSO	particle swarm optimization
SeATP	self-enhancing active transient protection
SLS	sea-level static
SM	surge margin
SS Op-Line	steady-state operating line
T4	turbine entry temperature
Wf	fuel flow
D_{rt}	deviation rate of thrust response time
J	objective function
$\hat{h}$	health parameters estimation
R_{rt}	recovery rate of thrust response time

t_r	response time
p	penalty function
y	measurements
$\hat{y}$	estimated measurements
Δ	delta
η	isentropic efficiency
Γ	flow capacity

subscript

acc	acceleration
cmd	command
dec	deceleration
max	maximum
min	minimum
pla	power level angle
ss	steady-state
tr	transient

1 Introduction

The existing industrial control system of gas turbine aero-engines still relies on the widely-used

sensor-based control strategies [1, 2]. However, due to the lack of on-board measurements for the performance parameter (i.e. thrust) and the safety-critical indicators (e.g. surge margin and turbine entry temperature) during transient engine states, indirect control approaches have to be implemented under industrial controller [3, 4]. As a common practice, low-pressure spool speed or engine pressure ratio are usually utilized to indirectly regulate thrust, while fuel schedule or rotor acceleration schedule must be applied to protect the engine from its physical limits, including surge limit, over-temperature limit, and blown-out limit, in a conservative way [5]. Additionally, degradation effects of gas turbine aero-engines over the life cycle are inevitable, which include blade surface changes (due to erosion, corrosion, or fouling) that influence blade aerodynamics [6, 7] and tip clearance increases that affect parasitic flows [8]. Unfortunately, the degradation effects, which worsen the health status of gas path components and engine performance, are still difficult to perceive [9]. As a result, a significantly conservative safety margin must be considered under the existing industrial engine control system using sensor-based strategies [10-12]. Engines regulated by the industrial controller are unavoidably subject to thrust variation [13], lower safety margin [14, 15], and poorer overall efficiency [16, 17] over the life span. Moreover, the next generation of aero-propulsion systems (e.g. Ultra High Bypass Ratio (UHBR) engines and Hybrid Electric Propulsion (HEP)) should be designed to deal with challenging targets of ultra-high efficiency and ultra-low emissions [18-20]. These ambitious targets also calls for an advanced control approach in addition to the marginal improvement in the engine component design and development. Model-based control strategy, in which unmeasured thrust, surge margin, and turbine entry temperature are directly controlled using an on-board engine model for real-time estimation with health status awareness of the engine, is considered as a promising solution to the

above-mentioned challenges regarding the conservatism reduction, performance enhancement of aircraft engines, and future aero-propulsion requirements [21].

Model-based control strategies for gas turbine aero-engines have attracted the attention of both industry and research institutes due to their potential in engine performance improvement and excessive safety margin reduction in control system design. The beginning of model-based control is mainly on nominal engines (i.e. clean engine or new engine performance) and limited gas path components degradations. Adibhatla et al. from General Electric (GE) pioneered the development of model-based control under the framework of intelligent engine control [22, 23]. They proposed different model-based control modes, including direct thrust control, direct surge margin control, and performance seeking control, and control model transition logic to reduce the unnecessary design margin and fuel consumption optimization. However, a reliable on-board engine model for unmeasured parameters estimation (e.g. thrust and surge margin) with desired fidelity was still hard to be achieved at that time. At the same time, Qi and Maccallum presented a model-based thrust control for a turbojet engine using an analytical thrust model [24]. Their simulation results confirmed that this model-based thrust control has effective thrust regulation capability even under inlet flow distortion. Unfortunately, the unavoidable degradation effects over the engine life cycle are not taken into account. The next step is the research carried by Kreiner and Lietzau from MTU Aero Engines on the direct surge margin control and direct turbine entry temperature control for turbofan engines [25, 26]. Virtual measurements of surge margin and turbine entry temperature from an observer-based on-board model are fedback to the control system and these model-based loops are augmented with the industrial baseline controller using sensor-based strategies. This control approach showed successful protection

of surge margin and turbine entry temperature for both new and degraded engines with limited degraded gas path components. Quinn et al. further employed model-based control in a hardware-in-loop platform of a turbofan engine simulator [27]. They demonstrated that model-based control is able to enhance thrust response under some degradation scenarios of scoped gas path components.

With the available access to on-board engine models accounting for all gas path components degradation over the engine life cycle, model-based control fascinates researchers in the gas turbine community again for the engine in-service performance improvement. Connolly et al. developed a model-based control architecture including surge margin and thrust control loop via the on-board engine model, optimal tuner Kalman filter (OTKF) [12]. Simulation results on a linear turbofan engine model confirmed that their proposed control configuration is beneficial for faster thrust response, compared to the industrial sensor-based controller when all the gas path components degrade with increasing flight cycles. Next, the same team further extended the model-based configuration with direct surge margin and thrust control to a nonlinear aero-thermal model for turbofan engines [28]. The simulations also verified the performance of the model-based controller regarding thrust response enhancement. A recent step by Connolly et al. is the exploration of model-based control strategies for design margin reduction of gas turbine aero-engines [29]. A lower surge margin was set in the model-based controller because the ability of the health situation perception from the on-board engine model for the regulated engine avoids the excessive safety margin. Their results showed that the model-based controller guarantees faster thrust response, higher overall efficiency, and optimized fuel consumption for the engine over the life cycle.

Unfortunately, based on the above-mentioned open literature, whether a flexible controller

parameters setting of a model-based controller for gas turbine aero-engines under degradation effects could further contribute to performance improvement of the engine is not yet known. Under this motivation, this study aims at pro-actively handling engine's transient safety limits (i.e. surge margin limit and turbine entry temperature limit) and thrust response improvement over the life cycle using model-based control strategies with updated control parameters. Self-enhancing active transient protection (SeATP) control using an on-board engine model is proposed in this paper. The SeATP controller is equipped with a bank of self-enhancing loops, aiming at thrust regulation and direct transient protection, whose controller parameters are updated periodically via an off-line global optimization approach over the life cycle of gas turbine aero-engines. This adaptable controller configuration intends to handle the transient operational limits of the engine in a pro-active manner and thrust response enhancement for degraded engines.

The remainder of this paper is organized as follows. Section two presents the details of gas turbine engine models, including a validated aero-thermal turbofan engine model for degradation simulations using publicly available degradation data and a verified on-board engine model concerned in this study. The development of an industrial baseline controller using sensor-based strategies for gas turbine aero-engines is explained in section three. Next, the SeATP controller is proposed and its structure is systematically described in section four. Finally, simulations are carried on the validated turbofan engine aero-thermal model to confirm the performance advantages of the proposed SeATP controller against baseline controller and active transient protection (ATP) controller during transient states under different degradation levels.

2 Gas turbine engine models

To verify the controllers developed in this paper, a dual-spool turbofan engine is examined here. In the following sub-sections, the details of the aero-thermal engine model for degradation simulations using publicly available data are firstly presented. Subsequently, a verified on-board engine model is briefly described.

2.1 Aero-thermal engine model

Gas turbine engines aero-thermal model could be served for faithful engine performance simulation. In this section, details of a validated aero-thermal model of a turbofan engine under nominal conditions (i.e. for clean or ideal performance) and the extension for degradation simulations using publicly available degradation data are presented.

The examined engine is a dual-spool, separate exhaust, fixed geometry turbofan engine with an intended application to general aircraft [30]. Major components in this engine are fan, high-pressure compressor (HPC), combustion chamber, high-pressure turbine (HPT), low-pressure turbine (LPT), bypass nozzle, and core nozzle. A gear box exists between fan and low-pressure spaft to achieve high bypass ratio. The only control variable of this engine is fuel flow (Wf). The schematic and the take-off specification of the engine at sea-level static (SLS) and international standard atmosphere (ISA) are shown in Fig. 1 and Table 1, respectively.

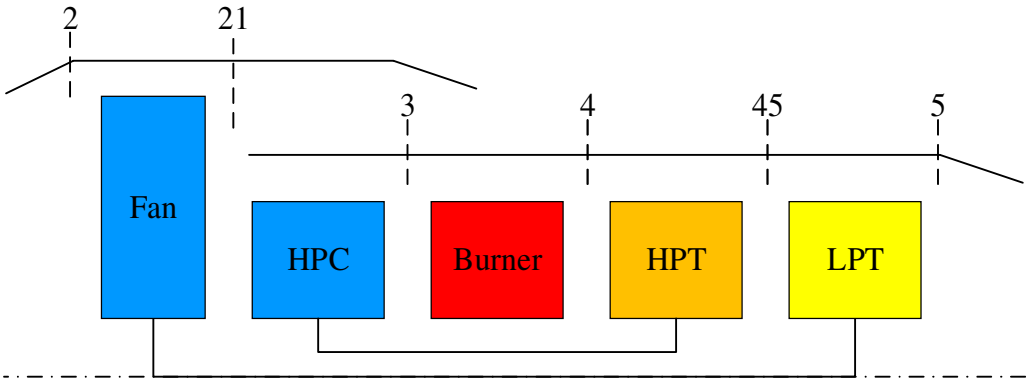

Fig. 1 Schematic of the examined dual-spool turbofan engine

Table 1 Take-off specification of the examined dual-spool turbofan engine [30]

Parameters	Values
Ambient temperature (K)	288.15
Ambient pressure (kPa)	101.325
Intake mass flow (kg/s)	13.68
Fan speed (rpm)	13323
High-pressure spool speed (rpm)	50990
Bypass ratio	6.83
Fan pressure ratio	1.20
High-pressure compressor pressure ratio	4.38
Turbine entry temperature (K)	1108
Fuel flow (kg/s)	0.036
Maximal thrust (kg)	246.48

An aero-thermal model of the examined turbofan engine was firstly developed to represent the engine's steady-state and transient performance under nominal conditions. This aero-thermal engine model is a physics-based model that is constructed by the component characteristic maps to guarantee the continuity of flow capacity and work balance. Modelling details could be referred to [31-34]. Validation of the nominal aero-thermal engine model can be found in the authors' previous study [3].

The next step is how to realistically replicate the degradation effects in the aero-thermal engine

model. Degradation on gas turbine engine performance is usually modelled by introducing health parameters for compressors and turbines, which represent the health status/deviation of major components in the gas path [14, 35, 36]. Therefore, degraded component maps could be obtained via the movement of their original clean maps based on these health parameters. Details of degradation modelling of gas turbine engines could be referred to our previous study [1, 3]. Additionally, the gas path components degradation data quantified by the National Aeronautics and Space Administration (NASA) based on in-service data from airliners, airframe manufacturers, and engine test results from JT9D turbofan engines, is utilized here, as shown in Table 2 [13, 37, 38]. In this table, the evolving trend of the health parameters, i.e. flow capacity ($\Delta\Gamma$) and isentropic efficiency ($\Delta\eta$) for all gas path components is given.

Table 2 Degradation data of turbofan engines quantified by NASA [13, 37, 38]

Flight cycle	$\Delta\eta_{Fan}$ (%)	$\Delta\Gamma_{Fan}$ (%)	$\Delta\eta_{HPC}$ (%)	$\Delta\Gamma_{HPC}$ (%)	$\Delta\eta_{HPT}$ (%)	$\Delta\Gamma_{HPT}$ (%)	$\Delta\eta_{LPT}$ (%)	$\Delta\Gamma_{LPT}$ (%)
0	0	0	0	0	0	0	0	0
3000	-1.50	-2.04	-2.94	-3.91	-2.63	+1.76	-0.54	+0.25

The health parameters of compressors (i.e. fan and HPC) and turbines (i.e. HPT and LPT) are defined in Eqs. (1)-(2),

$$\Delta\Gamma = \frac{\Gamma_{real} - \Gamma_{clean}}{\Gamma_{clean}} = \frac{\Gamma_{real}}{\Gamma_{clean}} - 1 \tag{1}$$

$$\Delta\eta = \eta_{real} - \eta_{clean} \tag{2}$$

where Γ_{real} and Γ_{clean} denote corrected flow capacity for degraded maps and clean maps of

compressors or turbines, respectively; η_{real} and η_{clean} are isentropic efficiency for degraded maps and clean maps of compressors or turbines.

2.2 On-board engine model

The model-based controller concerned in this study highly relies on a dependable on-board engine model. The Hybrid Wiener model (HWM), proposed in [3], is applied here as the on-board engine model. HWM endevours to estimate unmeasured safety-critical control parameters, i.e. thrust (F), surge margin (SM), and turbine entry temperature (T4) via monitoring the engine health status. The schematic of HWM, as the integration of on-line Wiener models and an off-line adaptation approach, is illustrated in Fig. 2. The off-line adaptation part serves to periodically update the nonlinear static blocks, i.e. steady-state engine operating line (SS Op-Line), of on-line Wiener models using the post-flight data (i.e. available measurements for rotor speed, gas path temperature and pressure) in order to match the particular degraded engine. Meanwhile, the on-line Wiener parts compute the unmeasured safety-critical parameters in a real-time manner. More modelling details of HWM and the validation results could be found in [3].

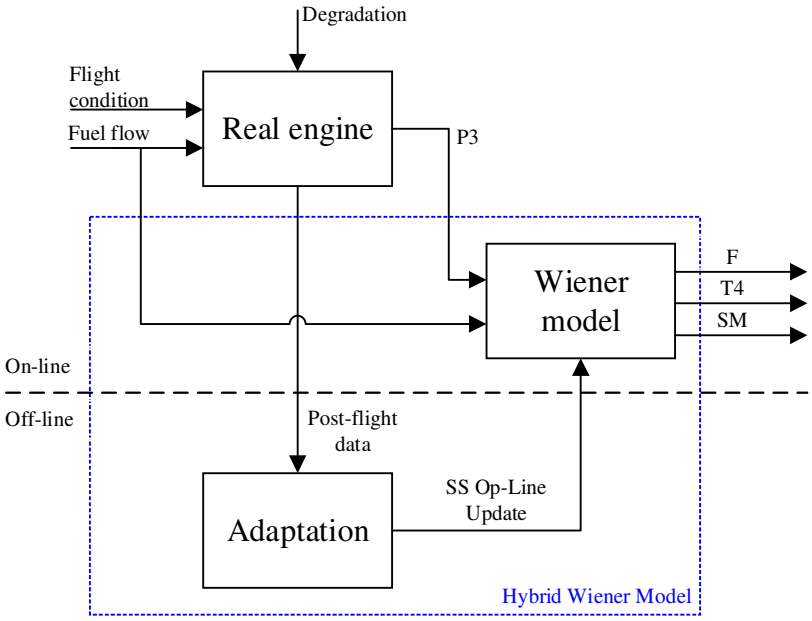

Fig. 2 Schematic of Hybrid Wiener model for on-board engine modelling

This on-board modelling technique is a methodological approach with the focus that the plant model over the life span could be updated periodically via the monitoring data. The philosophy behind this modelling method is promising for other power generating equipment considering inevitable in-service degradation effects.

3 Baseline controller design

The baseline controller implemented for the examined turbofan engine is the widely-used Min-Max sensor-based control configuration in gas turbine industry and research institutes [11, 26, 39], as illustrated in Fig. 3. Within this configuration, available engine measurements are feedback to a bank of steady-state loop and transient/limitation loops in order to provide the desired thrust response and

safely protect the engine from malfunctions. The steady loop takes advantage of gain-scheduling between engine pressure ratio (EPR) and fuel flow to hold the engine at a constant EPR level. This steady schedule is actually the steady-state operating line between EPR and fuel flow. The transient/limitation loops utilize the Min/Max selection logic to protect the engine from its physical limitations. EPR loop is constructed using EPR signal as a proxy of thrust. The acceleration loop limits the engine from its maximal core rotor acceleration to guarantee the engine within its surge limit and over-temperature limit during acceleration states, while the deceleration loop protects the engine from its blown-out boundary by limiting the maximal core rotor deceleration rate. Another two maximal rotor speed limitation loops are also implemented to prevent the engine from over-speed of low-pressure shaft (*N1max*) and high-pressure shaft (*N2max*) regarding structural limits.

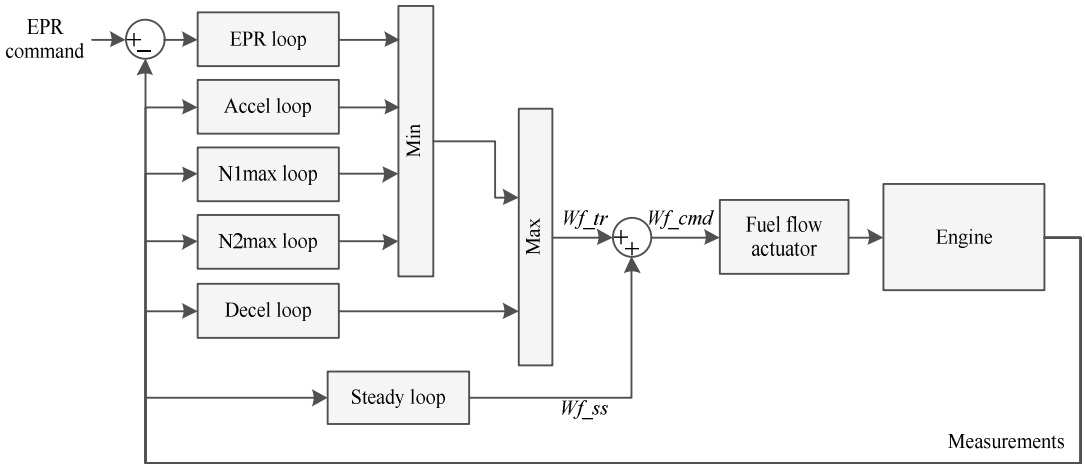

Fig. 3 Baseline controller configuration using sensor-based strategies for the target turbofan engine

The Min/Max selection logic and the fuel flow command to the fuel flow actuator are defined in Eqs. (4) and (5), respectively,

$$Wf_{tr} = \max(Wf_{dec}, \min(Wf_{EPR}, Wf_{acc}, Wf_{N_1 \max}, Wf_{N_2 \max})) \tag{3}$$

$$Wf_{cmd} = Wf_{tr} + Wf_{ss} \tag{4}$$

where Wf_{tr} is the winner of the transient/limitation loops; Wf_{EPR}, Wf_{acc}, Wf_{N1max}, Wf_{N2max}, and Wf_{dec} are the outputs from the EPR loop, acceleration loop, N1max loop, N2max loop, and deceleration loop, correspondingly. Therefore, the fuel flow command Wf_{cmd} to the fuel actuator is the sum of transient fuel flow Wf_{tr} and steady fuel flow Wf_{ss}, as shown in Eq. (4).

Each regulator in the transient/limitation loops is applied as a proportional-integral (PI) controller with anti-windup protection. Due to the inherent nature behind Min/Max strategy, only one control loop is active at a time. Therefore, the error between the actual value and limitation parameter in the in-active loops is inevitable and continuously integrated. This may lead to undesired interventions of some limitation loops even when the engine operates far away from the corresponding limit, which is known as integrator windup [40]. Fig. 4 illustrates the inner schematic of the EPR loop using PI controller with anti-windup protection as an example case. The main idea behind this setting is to decrease the input for the integrator when the specific loop is not active. A gain for integrator feedback (IFB) is augmented with an ordinary PI controller. The IFB gain acts on the mismatch between the fuel flow output from this loop (Wf_{EPR}) and the winner of Min/Max logic (Wf_{tr}) in the last time step. Proportional-integral-derivative (PID) control configurations are avoided for stability purposes in this study. Instead, as shown in Fig. 4, PI controllers with anti-windup logic, which are widely utilized by research institutes and manufacturers of gas turbine aero-engines[26, 40], are applied here.

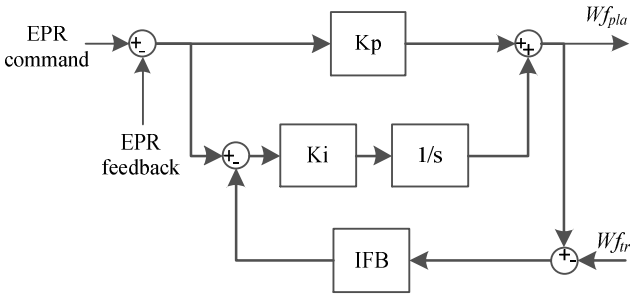

Fig. 4 PI controller with anti-windup protection in EPR loop

Particularly, an acceleration schedule and deceleration schedule have to be applied under the baseline controller for engine protection during transient states. This is due to the lack of available on-board measurements for surge margin, turbine temperature, and fuel-to-air ratio (FAR) in combustion chamber behind the baseline controller [40]. The acceleration schedule is established at each high-pressure shaft speed accounting for the surge margin limit of HPC and turbine entry temperature limit. Hence, a mapping between the maximum allowable rotor acceleration rate (N2dot) and high-pressure shaft speed (N2) could be obtained. Similarly, the deceleration schedule is developed at separated high-pressure shaft speed accounting for fuel-to-air ratio limit of combustion chamber to prevent the engine from blown-out. The transient operation limits of the examined turbofan engine, as displayed in Table 3, are applied here. Fig. 5 displays the resulted acceleration schedule, where parameters are normalized by their corresponding high-pressure shaft speed specified in Table 1. Hence, as can be seen in Fig. 6, the acceleration loop is formed using the acceleration schedule and PI controller with anti-windup logic to prevent the engine from surge and over-temperature. Under this acceleration loop configuration, N2 measurement is initially used to get the N2dot limit (i.e. maximum allowable N2dot) from the established acceleration schedule. Then, the error between N2dot limit and actual N2dot is sent to the PI controller for engine acceleration protection. In order to avoid oscillation in N2dot

calculation, a low-pass filter is applied. Conversely, the deceleration loop is developed in the same manner.

Table 3 Transient safety limits of the examined turbofan engine

Transient states	Limits	Value
Acceleration	Minimum HPC SM	15%
	Maximum T4	1195K
Deceleration	Minimum FAR	0.0206

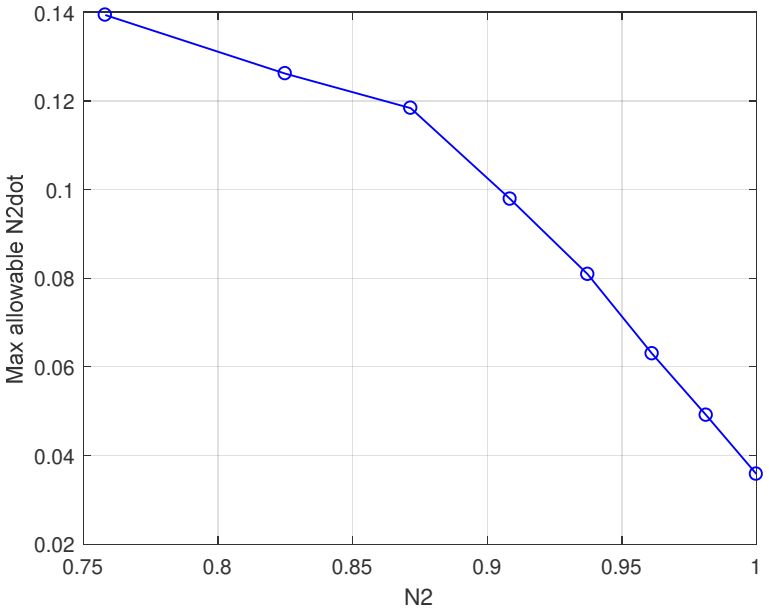

Fig. 5 Acceleration schedule for the target turbofan engine

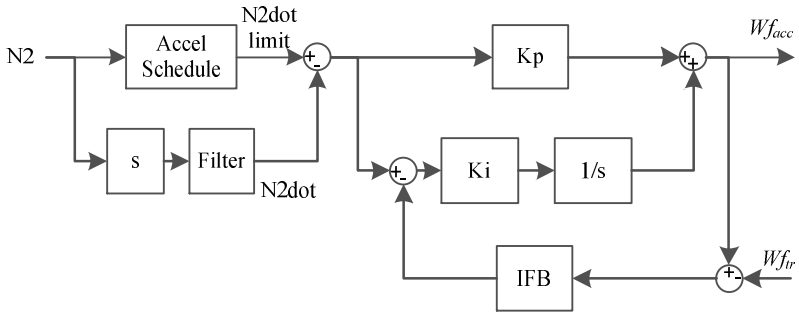

Fig. 6 Acceleration loop configuration

4 Self-enhancing model-based active transient protection controller design

As discussed in Section 3, the baseline controller using sensor-based strategies is not capable of pro-actively controlling the engine, especially during transient states. One point is that the baseline controller can only conservatively protect the engine from the transient limits via an in-direct approach, i.e. the acceleration and deceleration schedule. The other is that the inevitable degradation effects over the engine life cycle cannot be fully accounted in the transient schedules. Hence, self-enhancing active transient protection (SeATP) controller using model-based strategies is proposed in this section, which aims at improving the engine transient performance and pro-active handling of the engine operational limits.

4.1 SeATP architecture

SeATP controller is constructed with the integration of an on-line model-based controller and an off-line part for self-enhancing capability implementation, as illustrated in Fig. 7. The off-line part periodically updates the on-line model-based controller parameters using an optimization approach for degraded engines. Details of the off-line part are presented in Section 4.2.

The on-line part utilizes the Hybrid Wiener model (HWM), a faithful on-board engine model described in Section 2, to form a model-based controller. Virtual measurements for surge margin (SM) of HPC and turbine entry temperature (T4) from HWM could be directly feedback and controlled. SM and T4 are selected in this study because gas turbine engines run closer to their surge limit and over-

temperature limit during rapid acceleration states. Hence, surge margin loop and turbine entry temperature loop are developed in SeATP controller for engine acceleration protection, in place of the acceleration loop using in-direct rotor acceleration schedule behind baseline controller. Steady loop and other transients/limitation loops (i.e. EPR loop, deceleration loop, N1max loop, and N2max loop) remain the same as those in baseline controller, as depicted in Fig. 3. Min/Max selection strategy for transient/limitation loops is still applied for the SeATP controller.

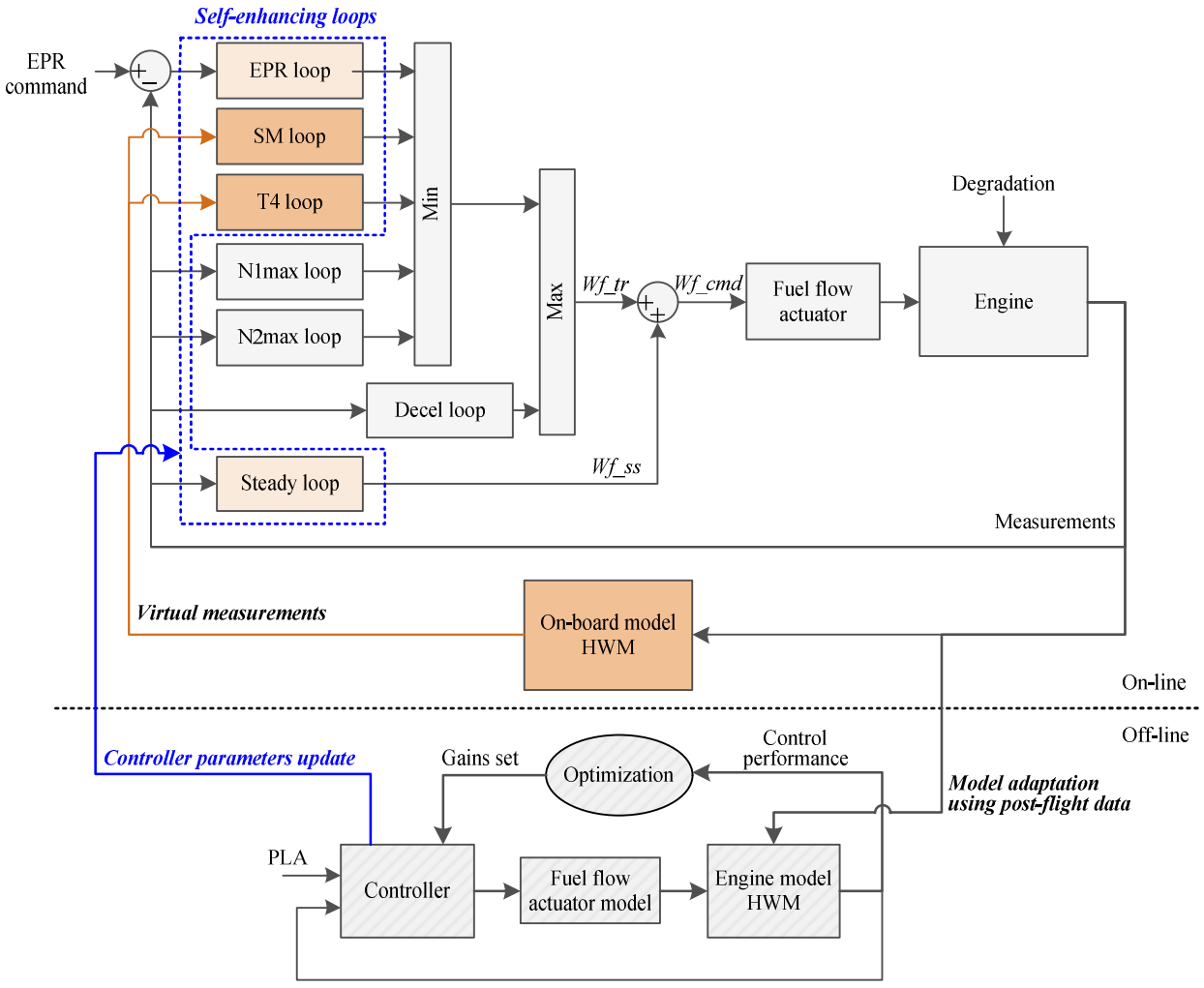

Fig. 7 Configuration of self-enhancing active transient protection controller

Therefore, the transient fuel flow and the fuel flow command behind SeATP controller are defined

in Eqs. (6) and (7), respectively,

$$Wf_{tr} = \max(Wf_{dec}, \min(Wf_{EPR}, Wf_{SM}, Wf_{T4}, Wf_{N_1 \max}, Wf_{N_2 \max})) \tag{5}$$

$$Wf_{cmd} = Wf_{tr} + Wf_{ss} \tag{6}$$

where Wf_{tr} is the winner of the transient/limitation loops; Wf_{EPR}, Wf_{SM}, Wf_{T4}, Wf_{N1max}, Wf_{N2max}, and Wf_{dec} are the outputs from EPR loop, surge margin loop, turbine entry temperature loop, N1max loop, N2max loop, and deceleration loop, respectively. Therefore, the fuel flow command Wf_{cmd} to the fuel actuator is the sum of transient fuel flow Wf_{tr} and steady fuel flow Wf_{ss}, as shown in Eq. (6).

The implementation of surge margin loop and turbine entry temperature loop is explained in the following sub-sections.

4.1.1 Surge margin loop

With the surge margin estimation, surge margin loop is therefore formed, as depicted in Fig. 8. A PI controller with anti-windup protection is employed. Therefore, the surge margin loop tries to protect the controlled engine away from its surge margin limit during acceleration states. The output from SM loop is the transient fuel flow of surge margin Wf_{SM}, which is then sent to Min/Max selection logic for engine protection. Details of the anti-windup protection logic can be referred to Fig. 4.

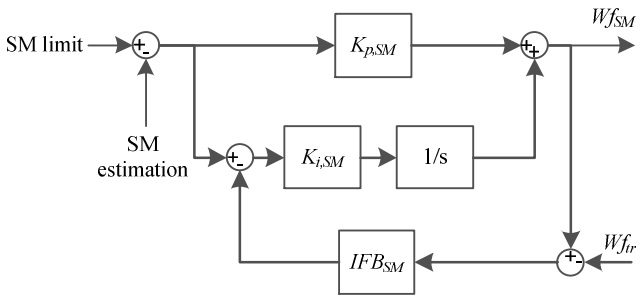

Fig. 8 Surge margin loop schematic

4.1.2 Turbine entry temperature loop

The turbine entry temperature loop is then formed similarly with the T4 estimation, as illustrated in Fig. 9. This loop endevours to directly protect the engine from its maximum T4 limit during acceleration states.

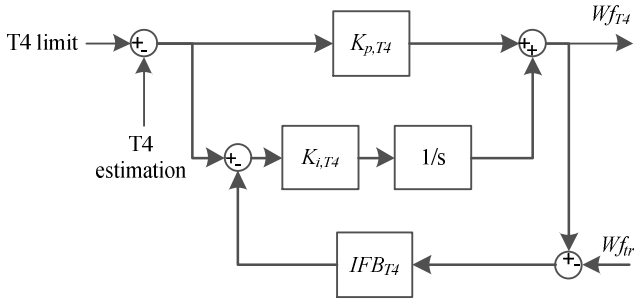

Fig. 9 Turbine entry temperature loop schematic

4.2 Self-enhancement capability implementation

With the inevitable degradation effects of gas turbine engines over the life cycle, degraded engines operate much closer to the surge limit and turbine entry temperature limit [3]. Therefore, self-enhancement capability implementation in an off-line manner is motivated for the proposed SeATP controller depicted in Fig. 7. This self-enhancement capability aims at proactively controlling the engine's transient operational limits via periodically updating the controller gains in transient loops and the steady loop parameters behind the SeATP controller.

The SeATP controller is realized by a bank of self-enhancing loops including transient loops and

the steady loop, as shown in Fig. 7. The transient loops incorporate the EPR loop, surge margin loop, and turbine entry temperature loop. The selection reason for these transient loops is that they have a significant influence on the engine acceleration performance, which is strictly specified in airworthiness regulations for civil aero-engines [41]. Details of the updating mechanism of the self-enhancing loops are presented in the following sub-sections.

4.2.1 Steady loop update

It has been demonstrated that gradual degradation effects mainly show an impact on the steady-state performance of gas turbine engines [3]. Consequently, the first attempt for the SeATP controller is to periodically update its steady loop parameters to match a particular degraded engine. The steady loop implemented in the SeATP controller is the engine steady-state operating line (SS Op-Line) between fuel flow (Wf_{ss}) and engine pressure ratio (ERP_{ss}), as defined in Eq. (8).

$$Wf_{ss} = f\left(EPR_{ss}\right) \tag{7}$$

Fig. 10 illustrates the steady loop update configuration by an off-line model adaptation approach using post-flight engine monitoring data. This is achieved by two steps. The first step is the health parameters estimation to track the gas path component performance due to degradation effects, while the second walk is to generate updated steady-state operating lines. In the first step, the steady-state measurements (i.e. under cruise state) in engine post-flight data during the previous flight cycle and the estimated measurement from the aero-thermal model form an objective function, as defined in Eq. (9), where y denotes steady-state measurements in post-flight engine data, $\hat{y}$ is the estimated

measurements from the aero-thermal model and M is the total number of measurements. Once the objective function is minimized, the accurate health parameters estimation $\hat{h}$ is therefore obtained. Finally, the updated SS Op-line is constructed by inserting the estimated health parameters into the aero-thermal engine model. More details of the off-line model update approach could be referred to [3]. With the updated SS Op-Line (i.e. steady fuel flow versus EPR), the steady loop in the SeATP controller is therefore reconstructed to match the particular engine.

$$J = \frac{1}{M}\sum_{i=1}^{M}\left|\frac{\hat{y}-y}{y}\right|\cdot 100 \tag{8}$$

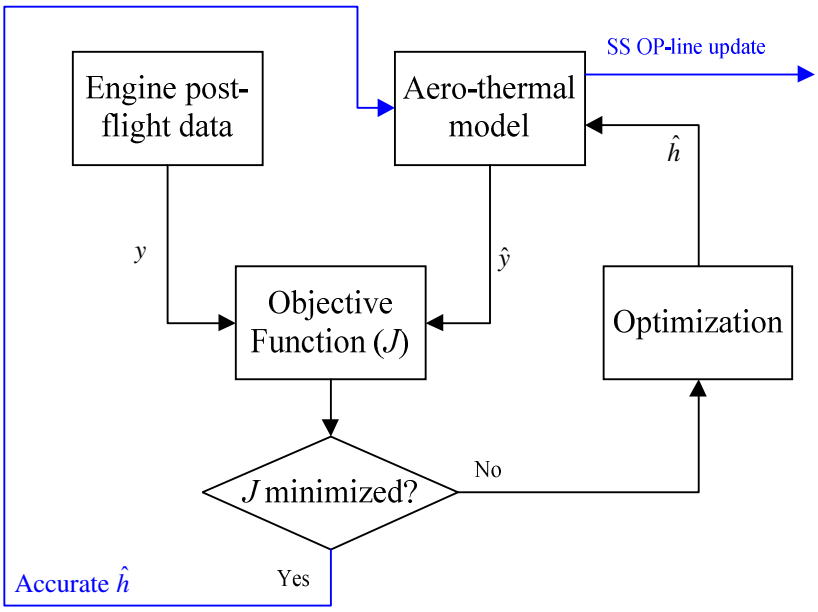

Fig. 10 Off-line model adaptation approach

4.2.2 Controller gains update

The next core feature behind SeATP controller is the controller gains update within the bank of

self-enhancing loops, as highlighted in Fig. 7. Corresponding loops are the EPR loop, surge margin loop, and turbine entry temperature loop, which own a strong coupling effect with the engine acceleration capability. The controller gains update in the off-line part is fulfilled by three steps: firstly, engine model adaptation for a specific degraded engine; secondly, closed-loop engine control system formation; thirdly, the controller gains optimization and update. Details of the off-line element behind the SeATP controller are presented as follows.

4.2.2.1 Engine model adaptation

The first step is the engine model adaptation for a particular controlled degraded engine, as depicted in the off-line part in Fig. 7. For fast execution considerations, the Hybrid Wiener model (HWM) with low computational burden and desirable fidelity for gas turbine engines modelling is also applied here as a control-oriented engine model. HWM utilizes post-flight engine monitoring data to adapt to a degraded engine. More details of HWM could be referred to [3].

4.2.2.2 Close-loop engine control system formation

The second footprint is the formation of closed-loop engine control system model in the off-line element behind SeATP controller. The adapted engine model (HWM) described in Section 4.2.2.1, fuel flow actuator model, and the controller block are integrated. The controller block here owns the same architecture as the on-line counterpart of the SeATP controller, as shown in Fig. 7. Specifically, a steady loop in combination of transient loops (EPR loop, surge margin loop, turbine entry temperature loop, and deceleration loop) and limitation loops (N1max loop and N2max loop) using Min/Max selection

logic exist in the off-line controller block. The steady loop here utilizes the updated steady-state engine operating line, as defined in section 4.2.1, to match an individual degraded engine.

4.2.2.3 Controller gains optimization

The third walk is controller gains optimization to enhance the transient performance of degraded engines. This is achieved based on the adapted engine model (HWM) and formation of closed-loop engine control system in the above-mentioned sub-sections. Since the thrust response of gas turbine engines is considerably affected by the controller parameters, the problem of transient performance improvement for gas turbine engines could be transformed into finding a set of optimized controller gains by the definition of control performance of interest. However, due to the nonlinearity and the switching feature in the Min/Max selection logic behind the SeATP controller, it is therefore motivated to tune the gains in all control loops simultaneously. Global optimization-based gain tuning approach, as a validated practice for the industrial baseline controller with multiple control loops of gas turbine engines [4, 5], is introduced here for the SeATP controller gains optimization for different flight cycles.

Self-enhancing loops, highlighted in Fig. 7, are concerned in this study, whose controller gains are optimized and updated periodically, including the transient loops (i.e. EPR loop, surge margin loop, and turbine entry temperature loop) and the steady loop. The parameters in the deceleration loop and limitation loops, including N1max/N2mas loops, are fixed for the nominal engine. Therefore, the controller gains in the self-enhancing loops (9 gains in total) could be optimized in an off-line manner after each flight cycle, in order to improve the engine performance.

The controller gains optimization is fulfilled by a pre-defined objective function for control

performance and safety concerns. A single-objective function is defined in Eq. (10),

$$J(gains) = t_r + \left(p_1 + p_2 + p_3 + p_4 \right) / 4 \tag{9}$$

where a performance item and penalty functions are formed. The performance item is normalized thrust response time t_r, which is specified as the response time of the controlled engine from idle to 95% maximum thrust [41]. The remaining parts in Eq. (9) are the penalty functions for the considerations of EPR tracking error, surge margin/turbine entry temperature protection, and the smooth switch between different loops. Table 4 indicates the specification of these penalty functions. All the items in the penalty functions are normalized in the range of [0, 1] to balance their importance.

Table 4 Specification of the penalty functions

Mathematical presentation	Significance of the penalty function
$p_1 = abs(EPR_{\max} - EPR_{cmd}) * 100$	Represents EPR tracking error at the maximum PLA value. E.g. 0.01 overshoot leads to p_1=1.
$p_2 = \begin{cases} 0, SM_{\min} \geq SM_{\text{limit}} \\ abs(SM_{\min} - SM_{\text{limit}}) * 50, SM_{\min} < SM_{\text{limit}} \end{cases}$	Represents the violation of surge margin limit. When the error is 0.02 if SM_{min}<SM_{limit}, p_2=1.
$p_3 = \begin{cases} 0, T_{4,\max} \leq T_{4,\text{limit}} \\ (T_{4,\max} - T_{4,\text{limit}}) * 100, T_{4,\max} > T_{4,\text{limit}} \end{cases}$	Represents the violation of over-temperature limit. When the error is 0.01 if $T_{4,max}$> $T_{4,limit}$, p_3=1.
$p_4 = \begin{cases} 1, \text{ undesirable EPR loop intervention in acceleration states} \\ 0, \text{ otherwise} \end{cases}$	Prevents undesirable EPR loop intervention during the transition from SM loop to T4 loop in acceleration states.

Particularly, the penalty function p_4 is designed to prevent undesirable EPR loop intervention during the transition from SM loop to T4 loop in rapid acceleration states, as defined in Table 4. Fig. 11 illustrates the undesirable EPR loop activation during acceleration states in the optimization process, as an example case. Based on the tuning experience for SeATP controller, an in-appropriate set of gains

results in this unnecessary EPR loop activation. This contributes to frequent switches within the transient loops. Hence, it is essential to define the penalty function p_4 in order to avoid this undesired phenomenon. The main idea behind p_4, as shown in Table 5, is to find whether there is an EPR loop activation between the first time step (t_{int}) of SM loop activation and the last time step (t_{end}) of the T4 loop activation.

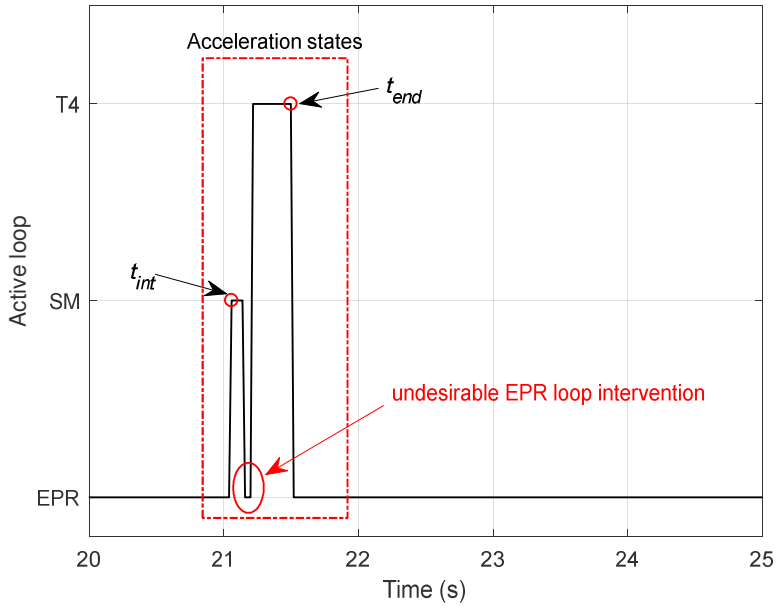

Fig. 11 Illustration of undesirable EPR loop intervention during acceleration states

Table 5 Implementation of the penalty function p_4

Algorithm: penalty function p_4	
Input	Active loop flag, simulation time
Process	
1.	Search the initial time step (t_{int}) when SM loop is active
2.	Search the ending time step (t_{end}) when T4 loop is active
3.	**if** there is an active flag of EPR loop between t_{int} and t_{end}
4.	$p_4 = 1$
5.	**else**
6.	$p_4 = 0$
7.	**end**
Output	Value of p_4

Apparently, smaller values of the performance item t_r and penalty parts p_1- p_4 will contribute to smaller objective function value and better control performance/safety considerations of the to-be-optimized controller for a target degraded engine. When the objective function defined in Eq. (9) is minimized, the optimized controller gains are found concerning the health status of degraded engines.

The optimized controller gains in combination of the updated steady loop parameters presented in Section 4.2.1 are integrated as controller parameters update for the controlled engine, as emphasized in Fig. 7. Consequently, SeATP controller is developed using the bank of self-enhancing loops with controller parameters update, which could be applied to the transient performance improvement and the pro-active handling of safety limits of the regulated engine in the next flight cycle. Details on the selected global optimization algorithm, optimization settings, and corresponding results are presented in Section 5.2.

5 Simulation results

To verify the proposed SeATP controller, numerical simulations on the validated turbofan engine aero-thermal model with degradation effects are carried. Three different controllers, the industrial baseline Min-Max controller, the active transient protection (ATP) controller, and the SeATP controller, are carefully examined and the obtained results are systematically compared. Table 6 indicates the settings for these tested controllers. The baseline controller owns fixed values for steady loop and

transient loop gains and is tuned on clean engines. SeATP controller could update the parameters in the self-enhancing loops, as presented in Section 4. Additionally, the ATP controller using the on-board engine model (HWM) is also placed here as a comparison basis, in which only steady loop parameters are updated with the increasing flight cycles while the transient loop gains are fixed for the nominal engine condition. Simulation comparisons of the examined different controllers are presented in this part.

Table 6 Setting comparison on the examined different controllers

Controller	Controller parameters	
	Steady loop parameters	Transient loop gains
Baseline	Fixed	Fixed
ATP	Updated	Fixed
SeATP	Updated	Updated (self-enhancing loops)

5.1 Case 1: ATP controller versus baseline controller

The baseline controller defined in Section 2 and the ATP controller presented in Table 6 are firstly compared on the validated aero-thermal engine model of the target turbofan engine, as depicted in Table 2. Fig. 12 displays the performance comparison between baseline controller and ATP controller from idle to full-power acceleration condition for both new engine and a severely degraded engine, namely at 3000 flight cycles (FC), at sea-level static situation. This aims to test the very harsh transient states in the take-off scenario. All the simulation outputs are normalized by their take-off specifications of the target engine, as defined in Table 1. The controller parameters behind the baseline controller and ATP controller were tuned on the nominal engine.

Fig. 12 (a) and (b) indicate that ATP controller owns faster thrust response than that of baseline controller for both new engine and the engine at 3000 flight cycles in view of engine pressure ratio (EPR) response and thrust response time. EPR is used as a thrust command and indicator for both baseline and ATP controller. The thrust response time is defined as the transient time from idle to 95% maximum thrust [41]. To quantify the thrust response improvement from the ATP controller, boost rate (*BR*) is defined in Eq. (11), in which $t_{r,ATP}$ and $t_{r,Baseline}$ denote the thrust response time from ATP controller and baseline controller, respectively. The thrust response time of the baseline controller and ATP controller from Fig. 12(b) are statistically documented in Table 7. It clearly demonstrates that ATP controller guarantees a 54.96% boost rate of thrust response time for the new engine, and even a 33.77% boost rate for the degraded engine at 3000 flight cycles, compared to the baseline controller. Regarding the baseline controller, it seems that a faster thrust response for 3000 cycle engine is observed than the new engine. This is due to the normalization approach, in which both the 95% maximum thrust and all the thrust response from different controllers are normalized with the maximum thrust of the new engine. However, degraded engines own a relatively larger initial steady thrust (e.g. 20-21s) compared with the new engine.

$$BR = \frac{t_{r,Baseline} - t_{r,ATP}}{t_{r,Baseline}} = 1 - \frac{t_{r,ATP}}{t_{r,Baseline}} \tag{10}$$

Table 7 Comparison on thrust response time between baseline and ATP controller

Engine	Response time, (s)		Boost rate, (%)
	Baseline	ATP	
New	2.42	1.09	54.96
3000FC	2.28	1.51	33.77

As can be observed from Fig. 12 (c) and (d), transient operational protection in view of surge margin and turbine entry temperature from both controllers is evaluated. Peak values of this simulation for SM and T4 are summarized in Table 8 accordingly. Although both controllers limit SM and T4 effectively from their safety boundaries, it can be seen that ATP controller operates the engines under both new and degraded conditions at 3000 flight cycles with a higher T4 maximum value and lower surge margin minimum value than those of baseline controller. Moreover, Fig. 12 (c) displays that the ATP controller takes the advantage of lower surge margin trajectories after the first peak surge margin value (i.e. between 21 s and 23 s) than that of the baseline controller for the engines under different degradation levels. ATP controller also regulates the engine for both new condition and degraded condition at higher T4 routes than that of the baseline controller. This undoubtedly contributes to the faster thrust response of the engine under ATP controller.

Table 8 Comparison on peak values of T4 and SM from the examined controllers

Controller	Maximum T4		Minimum SM	
	New	3000FC	New	3000FC
Baseline	1.008	1.069	0.1895	0.1740
ATP	1.035	1.070	0.1715	0.1728

Fig. 12(e) depicts the acceleration of high-pressure shaft (N2dot) of the control performance of both controllers in an alternative view. Apparently, ATP controller has a higher N2dot than that of the baseline controller in the middle stage of the acceleration states for the new engine and the degraded engine.

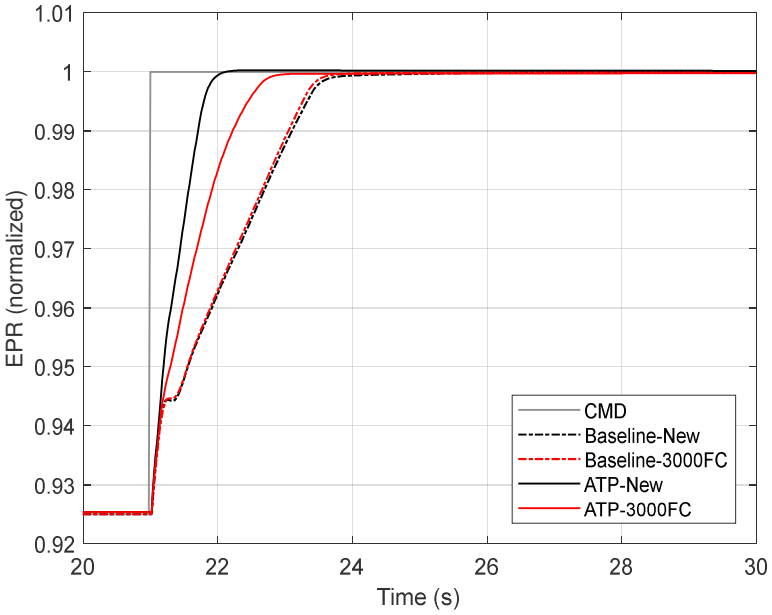

(a) Engine pressure ratio

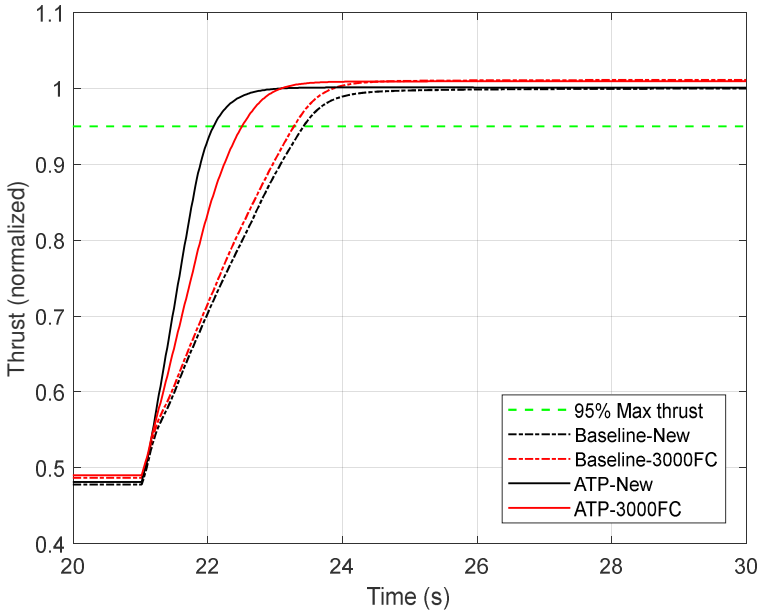

(b) Thrust

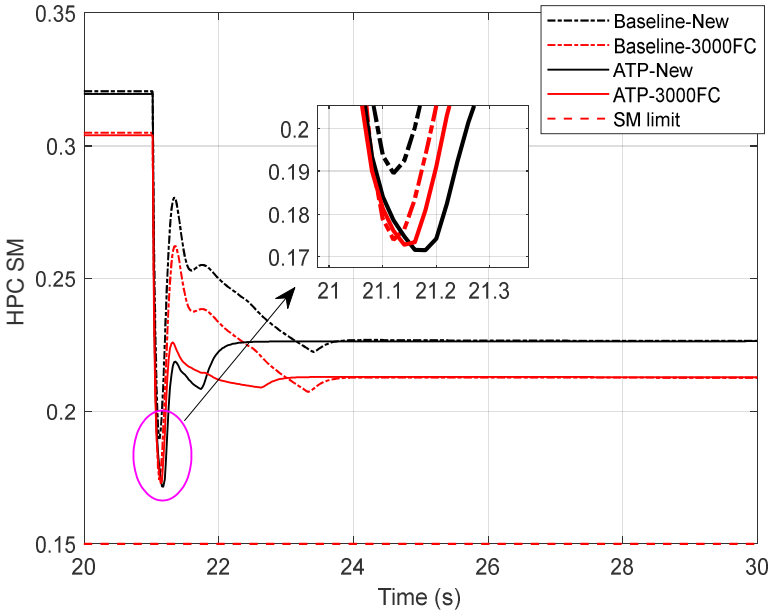

(c) HPC surge margin protection

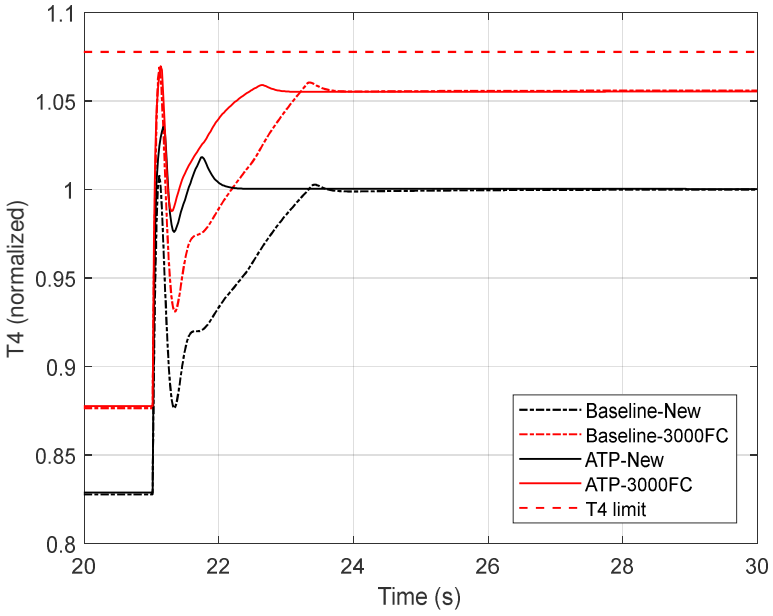

(d) Turbine entry temperature protection

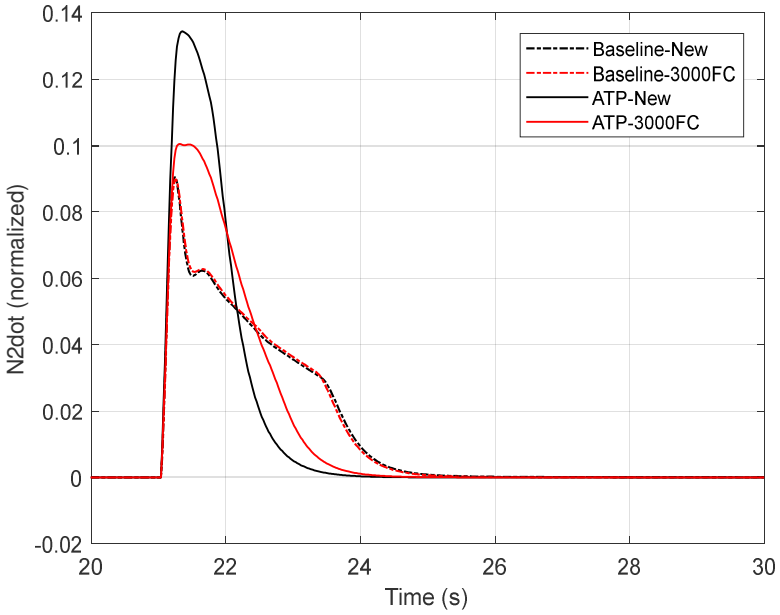

(e) High-pressure shaft speed acceleration

Fig. 12 Performance comparison of baseline controller and ATP controller for the examined engine during take-off acceleration states at different flight cycles

Measurements sent back to the controller are inherently subject to sensor noise. The baseline controller defined in Fig. 3. and the ATP controller described in Table 6 are implanted with certain levels of sensor noise, as listed in Table 9. Here, the control performance on the new engine from idle to full-power transient states is tested as a case study. Corresponding simulations results displayed in Fig. 13 clearly show that both the baseline controller and the ATP controller own sufficient robustness against sensor noise even during the rapid transient scenario. Moreover, the ATP controller using model-based strategies has much faster dynamic response, compared with the baseline controller, as illustrated in Fig. 13(a) and (b). Fig. 13(c) confirms that the dynamic behavior improvement is also from the higher N2dot during the middle stage of the transient test.

Table 9 Noise level of sensor measurements [42, 43]

Sensor	Symbol	Standard deviation (%)
Fan inlet temeprature	P2	0.25
HPC outlet pressure	P3	0.25
LPT outlet pressure	P5	0.25
Low-pressure shaft speed	N1	0.1
High-pressure shaft speed	N2	0.1
Fuel flow	Wf	0.2

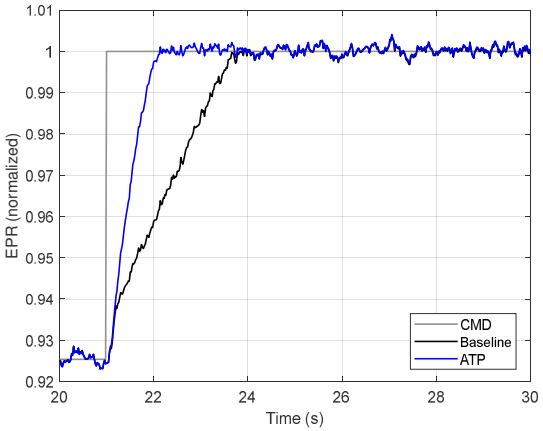

(a) Engine pressure ratio

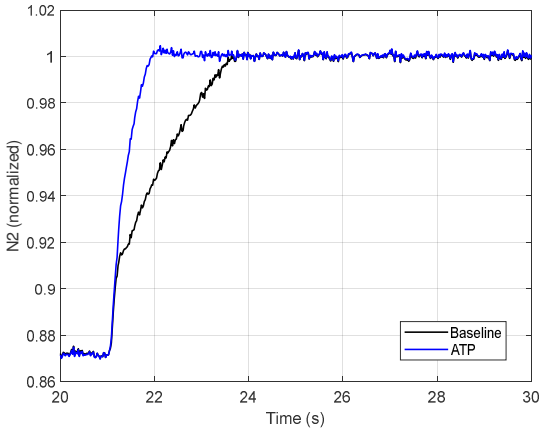

(b) high-pressure shaft speed

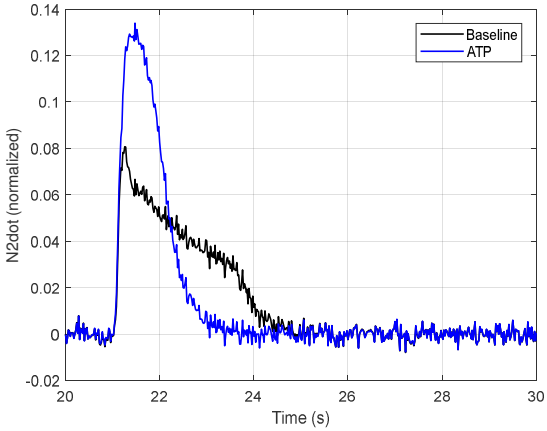

(c) Acceleration of high-pressure shaft

Fig. 13 Simulation results for the baseline controller and the ATP controller with sensor noise (the new engine from idle to full-power states)

Overall, ATP controller has a noticeable improvement of thrust response time for both the new engine and degraded engine, compared with the baseline controller. However, ATP controller shows an undesirable thrust response delay for degraded engines, as can be seen from Fig. 12(b). This calls for a more flexible controller parameters setting of the model-based ATP controller over the engine life cycle.

5.2 Case 2: SeATP controller versus ATP controller

The concept of the SeATP controller developed in Section 4, whose controller parameters are updated periodically over the engine life cycle is validated via numerical simulations on the turbofan engine aero-thermal model. Because it has confirmed that ATP controller outperforms the baseline controller regarding transient protection and thrust response enhancement, the SeATP controller is only compared with the ATP controller for degraded engines in this part.

Controller parameters update of SeATP controller for the examined turbofan engine at 3000 flight cycles is selected as a test case to represent a seriously degraded engine. As presented in Section 4.2, the SeATP controller is developed via steady loop update and controller gains update for the regulated degraded engine after the previous flight cycle (i.e. 2999 flight cycle). Particle swarm optimization (PSO) is chosen as a powerful optimization algorithm for the off-line gain tuning [44]. Table 10 illustrates the settings for the optimization of the gains by PSO. A total of 15 repeated runs is carried to deal with the repeatability of the optimization algorithm. Finally, the optimized gains set in combination with the updated steady loop parameters are transmitted to the engine control unit for the

next flight cycle.

Table 10 PSO settings for controller gains update

Setting	Value
Population size	50
Maximum generation	20
Repeated runs	15

As is observed from Fig. 14, the controller gains are optimized via the minimization of objective function value defined in Eq. (9) for the degraded engine. In this typical run, the fitness value of the objective function converges at the eighth generation, which is reached after the two noticeable decreases before this generation. Additionally, Table 12 shows the optimization results for the gains set. It is seen that the fitness value of SeATP controller has a observable decline compared to that of ATP controller for the specified degraded engine. The optimized gains set is shown in Table 11. Search bounds for each gain are defined by experimental experience for the examined engine. Moreover, the computational time of the averaged 15 runs are 20 mins and 49 secs under the platform with Core i5 processor and 8G memory. This averaged computation effort is affordable in the off-line optimization manner.

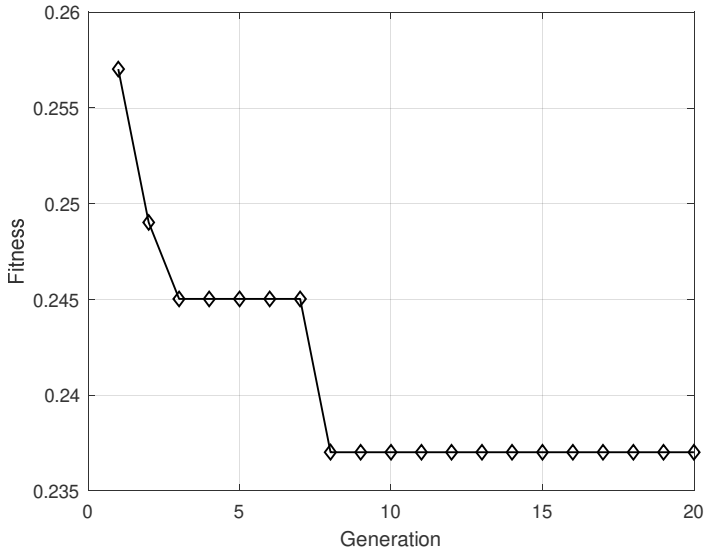

Fig. 14 Objective function convergence result of controller gains update for the examined engine at 3000 flight cycles

Table 11 Optimized controller gains for the examined degraded engine

Loop	Gains	Bounds	Value
EPR	$K_{p,EPR}$	[1.00, 7.00]	6.601
	$K_{I,EPR}$	[0.20, 0.40]	0.251
	IFB_{EPR}	[0.20, 0.40]	0.331
SM	$K_{p,SM}$	[0.88, 3.00]	1.479
	$K_{I,SM}$	[0.27, 0.33]	0.273
	IFB_{SM}	[0.40, 0.60]	0.410
T4	$K_{p,T4}$	[1.90, 3.00]	2.673
	$K_{I,\ T4}$	[0.40, 0.60]	0.401
	$IFB_{\ T4}$	[0.36, 0.44]	0.365

Table 12 Optimization results of the controller gains for the degraded engine

Controller	Fitness Value	Generation to achieve best solution	Averaged Computation time (min:sec)
ATP	0.2533	--	--
SeATP	0.2370	8	20:49

With the updated controller parameters, including the steady loop parameters and gains set in the self-enhancing loops, the SeATP controller is formed and tested on the turbofan engine aero-thermal model. Fig. 15 displays the performance comparison of SeATP controller and ATP controller for the examined engine at 3000 flight cycles from idle to full-power transient states under sea-level static condition.

Fig. 15 (a) and (b) show that SeATP controller has a significant improvement for thrust response time in view of engine pressure ratio and thrust for the target degraded engine. The thrust response time is also defined as the acceleration time from idle to 95% maximum thrust [41]. Moreover, two criterions to quantify the benefit of SeATP controller, i.e. deviation rate of thrust response time (D_{rt}) and recovery rate of thrust response time (R_{rt}), are defined in Eqs. (12) and (13), respectively,

$$D_{rt} = \frac{t_{r,deg} - t_{r,new}}{t_{r,new}} \tag{11}$$

$$R_{rt} = 1 - \frac{D_{rt,SeATP}}{D_{rt,ATP}} \tag{12}$$

where $t_{r,deg}$ and $t_{r,new}$ denote the thrust response time for degraded engines and new engines; $D_{rt,SeATP}$ and $D_{rt,ATP}$ are the thrust response time deviation rates from SeATP controller and ATP controller. Then, D_{rt} and R_{rt} for the examined controllers are documented in Table 13, based on results in Fig. 15 (b). It indicates that SeATP controller owns a much smaller D_{rt}, i.e. 13.23%, than that of ATP controller whose D_{rt} is 38.66% for the engine at 3000 flight cycles. Therefore, a considerable thrust response time recovery, i.e. 65.77%, is obtained by SeATP controller for the specified degraded engine.

Table 13 Thrust response time recovery from SeATP controller for the specified degraded engine

Controller	Response time, (s)		Deviation	Recovery
	New	3000FC	rate, (%)	rate, (%)
ATP	1.09	1.51	38.66	--
SeATP	--	1.23	13.23	65.77

Regarding the transient protection for surge margin and turbine entry temperature, Fig. 15 (c) and (d) show the advantages from the SeATP controller for the degraded engine. The results from both figures visibly confirm that SeATP controller regulates the degraded engine at a lower SM trajectory and a higher T4 route during this rapid transient states, compared to the ATP controller, due to the controller gains update and steady loop parameters update. Peak and valley values for T4 and SM from Fig. 15 (c) and (d) are recorded in Table 14 accordingly. It demonstrates that SeATP controller gets a higher second peak value for T4 and a lower second valley value than those of ATP controller, although both controller limits the degraded engine safely in the transient states. As also can be seen from Fig. 15 (f), T4 loop active time of SeATP controller is much shorter than ATP controller. The undesired longer activation time for T4 loop from ATP controller leads to the thrust response time delay for the degraded engine than that of the new engine. Additionally, Fig. 15 (e) shows the acceleration of high-pressure shaft which confirms that SeATP controller is able to operate the engine with a larger acceleration during the middle acceleration stage. This aspect also supports the capability from SeATP controller to enhance the thrust response, compared to ATP controller, for degraded engines.

Table 14 Peak/valley values comparison of T4 and SM of the examined controllers for target engine at 3000 flight cycles

Controller	T4 peak value		SM valley value	
	1st	2nd	1st	2nd
ATP	1.070	1.059	0.1728	0.2089
SeATP	1.062	1.067	0.1756	0.2026

Particularly, Fig. 15 (g) displays the comparison of the operating lines from SeATP controller and ATP controller on the high-pressure compressor map of the examined turbofan engine under this simulation. For clarification, both compressor maps for the new engine (i.e. clean map) and the degraded engine at 3000 flight cycles (i.e. degraded map) and the corresponding steady-state operating lines are plotted in this figure. It is observed that SeATP controller pro-actively regulates the specified degraded engine with a lower surge margin acceleration trajectory than that of ATP controller, especially above 0.90 corrected N2 speed, which indeed contributes to the thrust response enhancement depicted in Fig. 15 (b) and Table 13. The self-enhancing loops of SeATP controller is more compatible with the degraded engine so that the control performance is improved.

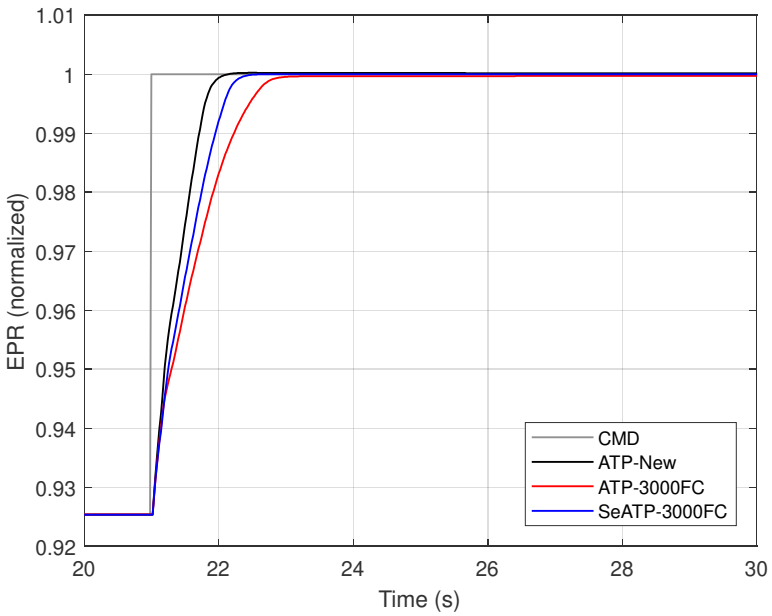

(a) Engine pressure ratio

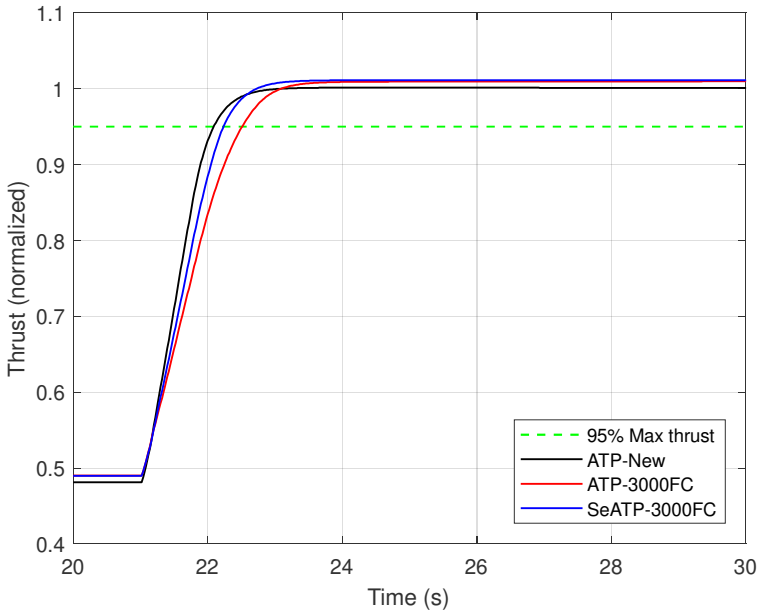

(b) Thrust

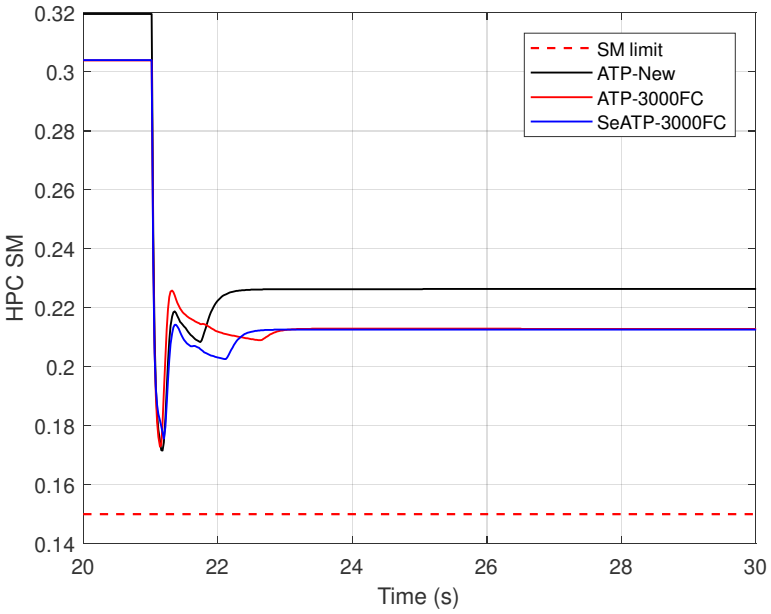

(c) HPC surge margin protection

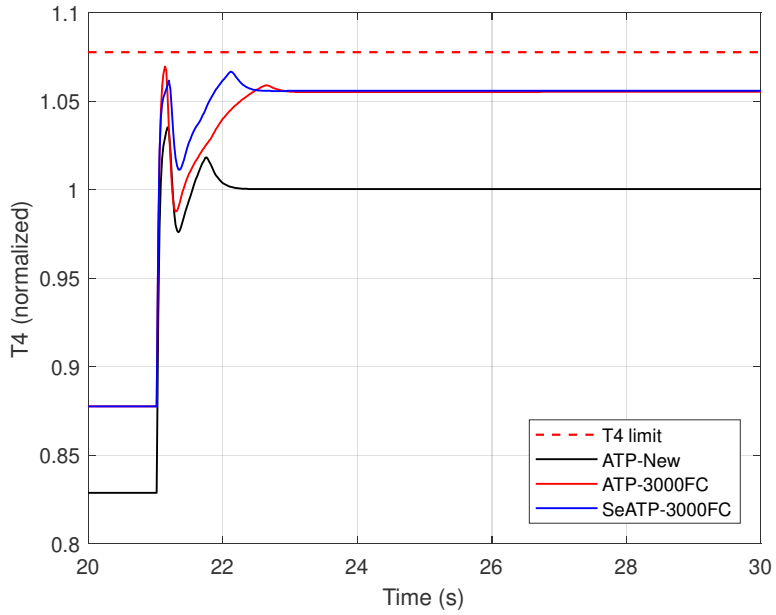

(d) Turbine entry temperature protection

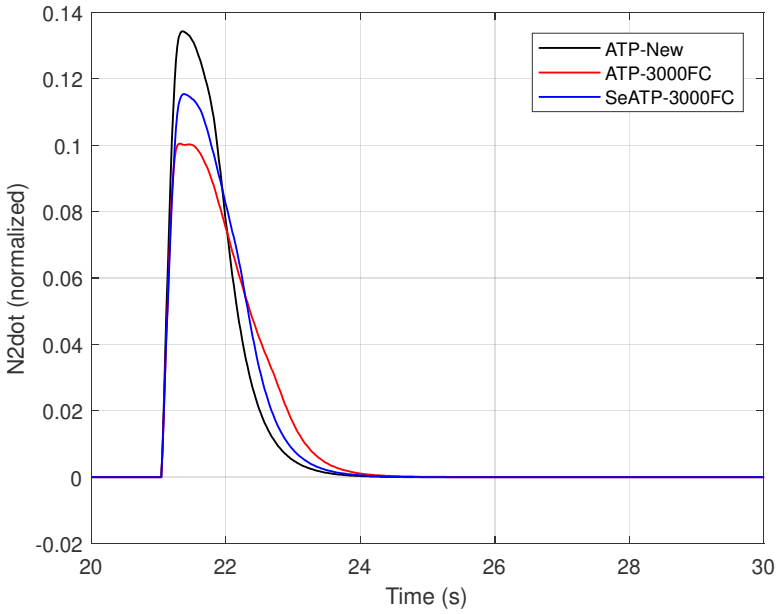

(e) Acceleration of high-pressure shaft speed

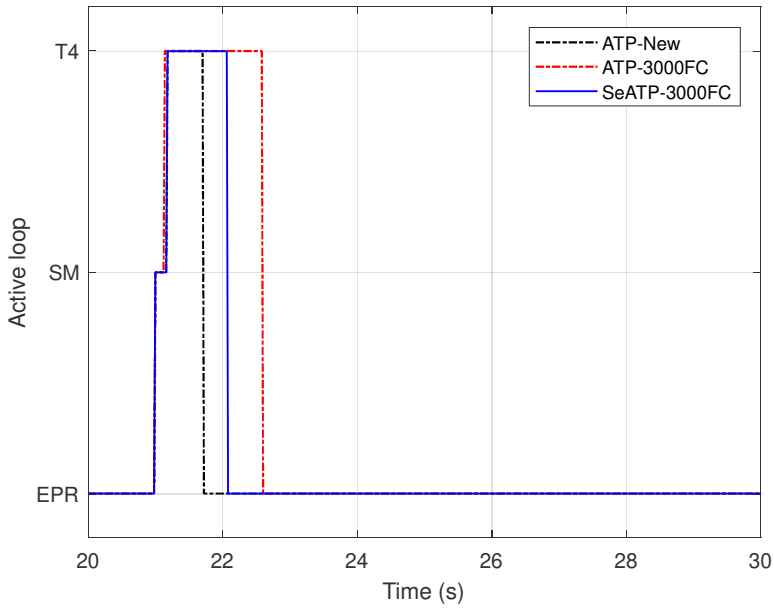

(f) Active loop

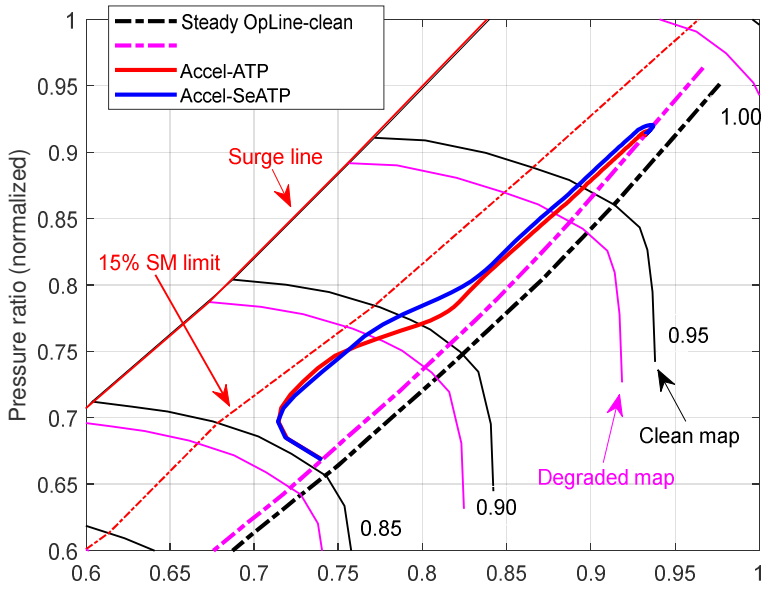

(g) Operating lines on HPC map

Fig. 15 Performance comparison of SeATP controller and ATP controller for the examined engine during take-off acceleration states at 3000 flight cycles

Furthermore, the SeATP controller and the ATP controller examined in this section are also embedded with sensor noise for practical considerations, as shown in Table 9. The severely degraded engine at 3000 flight cycles is selected as a test case. As can be seen from Fig. 16, simulation results from idle to full-power states demonstrate that the proposed SeATP controller and the ATP controller show effective control capabilities under sensor noise scenarios. Additionally, the transient performance enhancement from the SeATP controller for the degraded engine are validated, as depicted in Fig. 16(a) and (b). From Fig. 16(d), although both controllers are subject to multiple control loop switches at the end of the acceleration test, the proposed SeATP controller could still shorten the activation time of T4 protection loop.

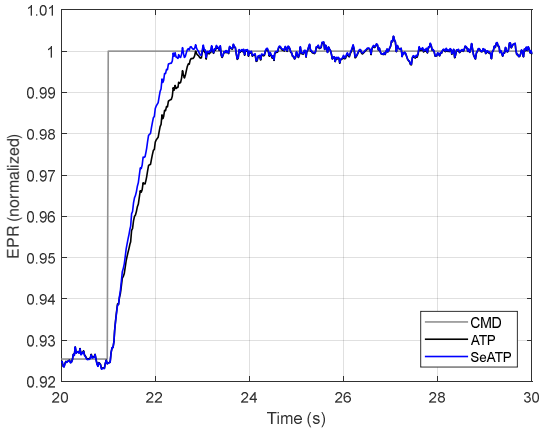

(a) Engine pressure ratio

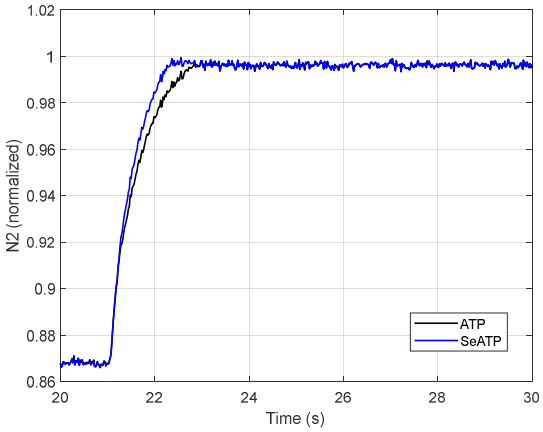

(b) High-pressure shaft speed

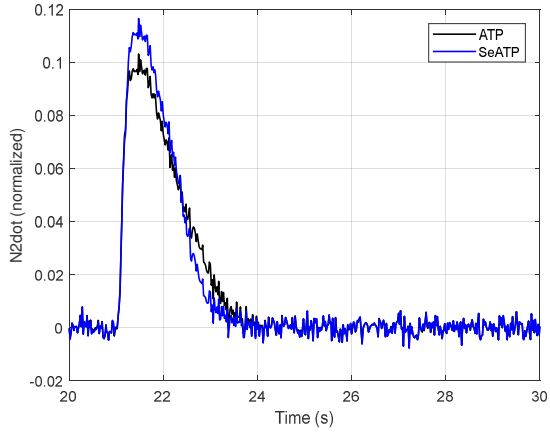

(c) Acceleration of high-pressure shaft

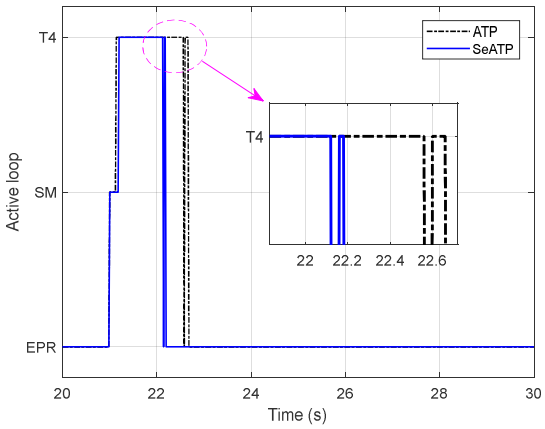

(d) Active loop

Fig. 16 Simulation results for the ATP controller and the SeATP controller with sensor noise (the degraded engine at 3000 flight cycles running from idle to full-power states)

For implementation purposes, a controller for gas turbine aero-engines is required to accommodate different flight phases [45]. The above-mentioned transient simulations on studied controllers are mainly carried at sea-level static conditions for the take-off scenario, in which both the engine and the control system endure critically harsh tests. The proposed SeATP controller in the study could be applied to other flight phases via the controller correction technique, which converts the controller parameters designed at sea-level states to other flight domains. More details on the controller correction method could be referred to [39].

5.3 Assessment of uncertainties on model-based controllers

Practically, gas turbine aero-engines at a specified flight cycle are subject to a statistical distribution of degradation variation. To validate the robustness performance of the studied controllers

against degradation uncertainties, random sampling analyses were carried on ATP controller and SeATP controller for degraded engines. Degradation variation bounds are set to ±10% of their values defined in Table 2, which are subsequently converted to a normal distribution with corresponding standard deviation and mean value for each health parameter of gas path components [46]. A total of 1000 repeated times of random sampling degradation variations for the engine with ATP controller and SeATP controller at 3000 flight cycles during the same idle to full-power transient states, as shown in Fig. 15, is tested. Fig. 17 indicates the robustness analysis results of the examined controllers regarding the scattering of minimum HPC surge margin and maximum turbine entry temperature in these transient states. It is also seen from Table 15, which is statistically recorded based on Fig. 17, that SeATP controller owns a significant decrease in the standard deviation of minimum SM and maximum T4, compared with those of ATP controller for the degraded engines. This confirms the better robustness performance of SeATP controller for degraded engines.

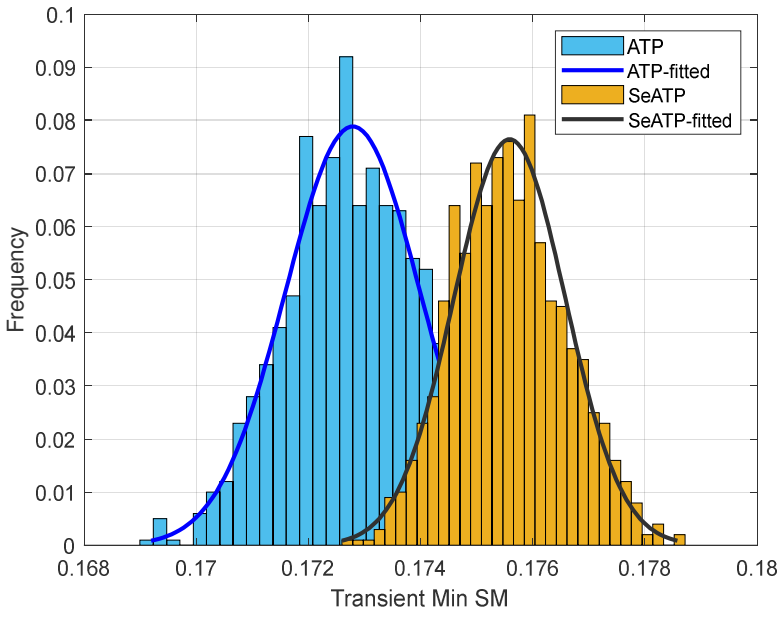

(a) Minimum HPC surge margin in transient states

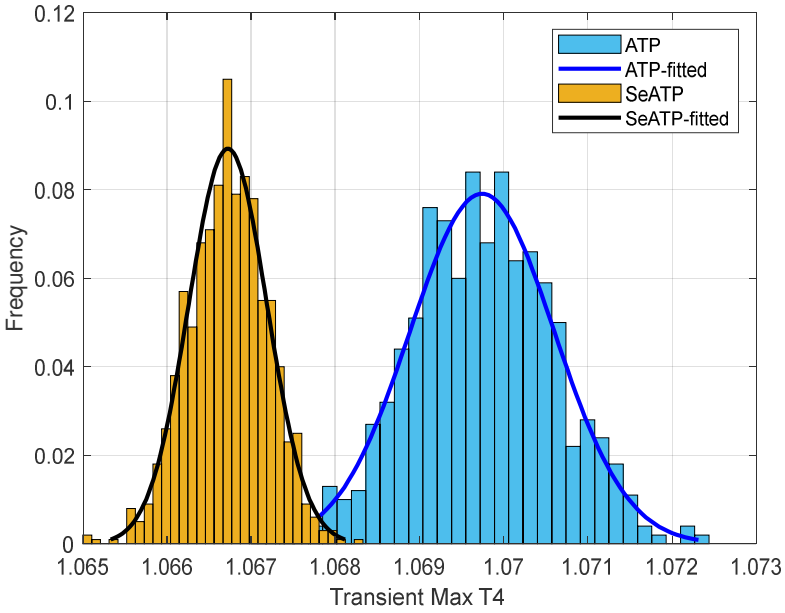

(b) Maximum turbine entry temperature in transient states

Fig. 17 Robustness analysis of SeATP controller and ATP controller for the examined engines at 3000 flight cycles

Table 15 Robustness evaluation statistics for the examined controllers against degradation variation

Controller	SM min		T4 max	
	Mean	Standard deviation	Mean	Standard deviation
ATP	0.1728	0.0012	1.0697	8.57e-4
SeATP	0.1756	9.96e-4	1.0667	4.64e-4

Above all, the control performance of SeATP controller is verified on the validated turbofan engine aero-thermal model. Compared to ATP controller with fixed gains, SeATP controller with both controller gains update and steady loop parameters update in the self-enhancing loops owns two significant benefits for degraded engines. One point is that SeATP controller can regulate the transient operational limits (i.e. surge margin limit and turbine entry temperature limit) more actively. The other

aspect is that a considerable recovery rate for thrust response time can be obtained by SeATP controller due to its compatibility to the degrade engine.

6 Conclusions

In this paper, self-enhancing active transient protection (SeATP) control is proposed for gas turbine aero-engines over the life cycle, which aims at pro-actively handling the transient operational limits and the thrust response improvement. SeATP controller is fulfilled by the integration of an on-line model-based control strategy using a verified on-board engine model (Hybrid Wiener model) and an off-line self-enhancement capability implementation. The key characteristic of the on-line block behind SeATP controller are a bank self-enhancing loops, including engine pressure ratio loop, surge margin loop, turbine entry temperature loop, and the steady loop, in which the controller parameters are updated periodically with the increasing flight cycles. Meanwhile, the off-line element of SeATP controller is responsible for the update of the corresponding controller parameters in the self-enhancing loops via a global optimization approach.

Numerical simulations for SeATP controller are carried on the validated turbofan engine aero-thermal model using publicly available degradation data. The other two controllers, i.e. the industrial sensor-based baseline controller and the model-based active transient protection (ATP) controller with fixed controller gains, are also examined as a comparison basis. The first simulation comparison results between baseline controller and ATP controller demonstrate that ATP controller owns a 54.96% boost

rate and even a 33.77% boost rate of thrust response time for the new engine and for the severely degraded engine at 3000 flight cycles, respectively, during the idle to full-power transient states at sea-level static condition. The second simulation case confirms that, for the specified degraded engine during the same idle to full-power acceleration test, SeATP controller with the bank of self-enhancing loops just has a 13.23% deviation rate of thrust response while ATP controller is subject to a noticeable 38.66% deviation rate of thrust response, compared to the thrust response time of the new engine under ATP controller. This means that SeATP controller ensures a considerable 65.77% recovery rate of thrust response deviation caused by ATP controller for degraded engines. The reason behind this thrust response improvement is due to the pro-active handling of surge margin limit and turbine entry temperature limit from the controller gains update of SeATP controller. Specifically, a lower transient surge margin trajectory and a higher turbine entry temperature route is realized by SeATP controller than those of baseline controller and ATP controller, while all the transient operational limits are effectively regulated. The robustness performance of SeATP controller against degradation variations are also validated regarding a considerable decrease in the standard variation of the minimum surge margin and maximum turbine entry temperature in transient states, compared with ATP controller. Therefore, the excellent control performance of SeATP controller for degraded engines is guaranteed. In future steps, the extension to the full flight envelope of the proposed SeATP controller as well as the application on other gas turbine engines configuration (e.g. large turbofan engines and ultra-high bypass turbofans) are areas of on-going investigations.

Reference

[1] Z. Wei, S. Zhang, S. Jafari, T. Nikolaidis, Gas turbine aero-engines real time on-board modelling: A review, research challenges, and exploring the future, Prog. Aerosp. Sci., 121 (2020) 100693.
[2] S. Jafari, T. Nikolaidis, Meta-heuristic global optimization algorithms for aircraft engines modelling and controller design; A review, research challenges, and exploring the future, Prog. Aerosp. Sci., 104 (2019) 40-53.
[3] Z. Wei, S. Jafari, S. Zhang, T. Nikolaidis, Hybrid Wiener model: An on-board approach using post-flight data for gas turbine aero-engines modelling, Appl. Therm. Eng., 184 (2021) 116350.
[4] Y. Liu, S. Jafari, T. Nikolaidis, Advanced optimization of gas turbine aero-engine transient performance using linkage-learning genetic algorithm: Part I, building blocks detection and optimization in runway, Chin. J. Aeronaut., 34 (2020) 526-539.
[5] M. Montazeri-Gh, S. Jafari, Evolutionary Optimization for Gain Tuning of Jet Engine Min-Max Fuel Controller, J. Propul. Power, 27 (2011) 1015-1023.
[6] D. Zhou, Q. Yao, H. Wu, S. Ma, H. Zhang, Fault diagnosis of gas turbine based on partly interpretable convolutional neural networks, Energy, 200 (2020) 117467.
[7] M. Kiaee, A.M. Tousi, Vector-based deterioration index for gas turbine gas-path prognostics modeling framework, Energy, 216 (2021) 119198.
[8] S. Kim, A new performance adaptation method for aero gas turbine engines based on large amounts of measured data, Energy, 221 (2021) 119863.
[9] Y.-Z. Chen, X.-D. Zhao, H.-C. Xiang, E. Tsoutsanis, A sequential model-based approach for gas turbine performance diagnostics, Energy, 220 (2021) 119657.
[10] C. Wang, Y.G. Li, B.Y. Yang, Transient performance simulation of aircraft engine integrated with fuel and control systems, Appl. Therm. Eng., 114 (2017) 1029-1037.
[11] H.A. Spang III, H. Brown, Control of jet engines, Control Eng. Pract., 7 (1999) 1043-1059.
[12] J. Connolly, A. Chicatelli, S. Garg, Model-Based Control of an Aircraft Engine using an Optimal Tuner Approach, Aiaa/asme/sae/asee Joint Propulsion Conference & Exhibit, 2012, pp. AIAA 2012-4257.
[13] J.S. Litt, K.I. Parker, S. Chatterjee, Adaptive gas turbine engine control for deterioration compensation due to aging, NASA/TM-2003-212607, 2003.
[14] S. Garg, Aircraft Turbine Engine Control Research at NASA Glenn Research Center, J. Aerosp. Eng., 26 (2013) 422-438.
[15] Z.S. Spakovszky, J.B. Gertz , O.P. Sharma, J.D. Paduano , A.H. Epstein , E.M. Greitzer, Influence of Compressor Deterioration on Engine Dynamic Behavior and Transient Stall-Margin, J. Turbomach., 122 (1999) 477-484.
[16] S. Tang, H. Tang, M. Chen, Transfer-learning based gas path analysis method for gas turbines, Appl. Therm. Eng., 155 (2019) 1-13.
[17] M. Bai, J. Liu, J. Chai, X. Zhao, D. Yu, Anomaly detection of gas turbines based on normal pattern extraction, Appl. Therm. Eng., 166 (2020) 114664.
[18] K. Ranasinghe, K. Guan, A. Gardi, R. Sabatini, Review of advanced low-emission technologies

for sustainable aviation, Energy, 188 (2019) 115945.
[19] D. Sziroczak, I. Jankovics, I. Gal, D. Rohacs, Conceptual design of small aircraft with hybrid-electric propulsion systems, Energy, 204 (2020) 117937.
[20] A. Dinc, NOx emissions of turbofan powered unmanned aerial vehicle for complete flight cycle, Chin. J. Aeronaut., 33 (2020) 1683-1691.
[21] S. Adibhatla, S. Garg, S. Griffith, K. Karnofski, N. Payne, B. Wood, Propulsion Control Technology Development Roadmaps to Address NASA Aeronautics Research Mission Goals for Thrusts 3a and 4, 2018 Joint Propulsion Conference, 2018, pp. 4732.
[22] S. ADIBHATLA, H. BROWN, Z. GASTINEAU, Intelligent engine control (IEC), 28th Joint Propulsion Conference and Exhibit, 1992, pp. 3484.
[23] S. Adibhatla, T. Lewis, Model-based intelligent digital engine control (MoBIDEC), 33rd Joint Propulsion Conference and Exhibit, 1997, pp. 3192.
[24] O.F. Qi, N.R.L. Maccallum, A Model-Based Approach to the Control of an Aircraft Gas Turbine Engine, ASME 1993 International Gas Turbine and Aeroengine Congress and Exposition, 1993, pp. 93-GT-402.
[25] K. Lietzau, A. Kreiner, Model based control concepts for jet engines, ASME Turbo Expo 2001: Power for Land, Sea, and Air, American Society of Mechanical Engineers, 2001, pp. 2001-GT-0016.
[26] A. Kreiner, K. Lietzau, The use of onboard real-time models for jet engine control, Project Report OBIDICOTE, MTU Aero Engines, Munich, Germany, 2000.
[27] R. Quinn, J. Sims, A. Behbahani, K. Semega, Improved turbine engine performance, responsiveness, and prognostics using model-based control in a hardware-in-the-loop simulation, 43rd AIAA/ASME/SAE/ASEE Joint Propulsion Conference & Exhibit, 2007, pp. 5712.
[28] J.W. Connolly, J. Csank, A. Chicatelli, J. Kilver, Model-Based Control of a Nonlinear Aircraft Engine Simulation using an Optimal Tuner Kalman Filter Approach, Aiaa/asme/sae/asee Joint Propulsion Conference, 2013, pp. AIAA 2013-4002.
[29] J.W. Connolly, J. Csank, A. Chicatelli, Advanced Control Considerations for Turbofan Engine Design, 52nd AIAA/SAE/ASEE Joint Propulsion Conference, 2016, pp. AIAA 2016-4653.
[30] M.V. Culmone, N. Garcia-Rosa, X. Carbonneau, Sensitivity Analysis and Experimental Validation of Transient Performance Predictions for a Short-Range Turbofan, ASME Turbo Expo 2016: Turbomachinery Technical Conference and Exposition, 2016, pp. GT2016-57257.
[31] P.P. Walsh, P. Fletcher, Gas turbine performance, John Wiley & Sons2004.
[32] J. Zhang, H. Tang, M. Chen, Linear substitute model-based uncertainty analysis of complicated non-linear energy system performance (case study of an adaptive cycle engine), Appl. Energy, 249 (2019) 87-108.
[33] J. Zhang, H. Tang, M. Chen, Robust design of an adaptive cycle engine performance under component performance uncertainty, Aerosp. Sci. Technol., (2021) 106704.
[34] J. Zhang, P. Dong, H. Tang, J. Zheng, J. Wang, M. Chen, General Design Method of Control Law for Adaptive Cycle Engine Mode Transition, AIAA Journal, (2021) 1-15 https://doi.org/10.2514/2511.J060674.
[35] A.J. Volponi, Gas turbine engine health management: past, present, and future trends, J. Eng. Gas Turbines Power, 136 (2014) 051201.

[36] S. Kim, K. Kim, C. Son, A new transient performance adaptation method for an aero gas turbine engine, Energy, 193 (2020) 116752.
[37] G. Sallee, Performance deterioration based on existing (historical) data; JT9D jet engine diagnostics program, Report No.: NASA-CR-135448, Pratt and Whitney, East Hartford, CT, 1978.
[38] G. Sallee, Performance deterioration based on in-service engine data: JT9D jet engine diagnostics program, Report No.: NASA-CR-159525, Pratt and Whitney, East Hartford, CT, 1979.
[39] Y. Liu, S. Jafari, T. Nikolaidis, Advanced optimization of gas turbine aero-engine transient performance using linkage-learning genetic algorithm: Part II, optimization in flight mission and controller gains correlation development, Chin. J. Aeronaut., 34 (2020) 568-588.
[40] J. Csank, R. May, J. Litt, T.-H. Guo, Control design for a generic commercial aircraft engine, 46th AIAA/ASME/SAE/ASEE Joint Propulsion Conference & Exhibit, 2010, pp. 6629.
[41] EASA. Certification specifications for engines CS-E amendment-4, European Aviation Safety Agency, 2015.
[42] G.L. Merrington, Fault Diagnosis of Gas Turbine Engines From Transient Data, J. Eng. Gas Turbines Power, 111 (1989) 237-243.
[43] V. Zaccaria, A.D. Fentaye, M. Stenfelt, K.G. Kyprianidis, Probabilistic Model for Aero-Engines Fleet Condition Monitoring, Aerospace, 7 (2020) 66.
[44] M. Montazeri-Gh, S. Jafari, M.R. Ilkhani, Application of particle swarm optimization in gas turbine engine fuel controller gain tuning, Eng. Optim., 44 (2012) 225-240.
[45] I.M.A. Ibrahem, O. Akhrif, H. Moustapha, M. Staniszewski, Nonlinear generalized predictive controller based on ensemble of NARX models for industrial gas turbine engine, Energy, 230 (2021) 120700.
[46] E. Tsoutsanis, N. Meskin, M. Benammar, K. Khorasani, A dynamic prognosis scheme for flexible operation of gas turbines, Appl. Energy, 164 (2016) 686-701.

Self-enhancing model-based control for active transient protection and thrust response improvement of gas turbine aero-engines

Wei, Zhiyuan

2021-12-29

Wei Z, Zhang S, Jafari S, Nikolaidis T. (2022) Self-enhancing model-based control for active transient protection and thrust response improvement of gas turbine aero-engines. Energy, Volume 242, March 2022, Article number 123030

https://doi.org/10.1016/j.energy.2021.123030